ACS OMEGA

http://pubs.acs.org/journal/acsodf

Article

Morphology-Tuned Electrochemical Immunosensing of a Breast Cancer Biomarker Using Hierarchical Palladium Nanostructured Interfaces

Anju Joshi, Anil Vishnu G K, Dhananjay Dhruv, Vishnu Kurpad, and Hardik J. Pandya*

Cite This: *ACS Omega* 2022, 7, 34177−34189

Read Online

ACCESS | Metrics & More | Article Recommendations | Supporting Information

ABSTRACT: Metallic nanostructures are considered attractive candidates for designing novel biosensors due to their enormously significant surface area, accelerated kinetics, and improved affinity. Controllable morphological tuning of metallic nanostructures on sensing interfaces is crucial for attaining clinically relevant sensitivity and exquisite selectivity in a complex biological environment. Therefore, a facile, convenient, and robust one-step electroreduction method was employed to develop different morphological variants of palladium (Pd) nanostructures supported onto oxidized carbon nanotubes to facilitate label-free electrochemical immunosensing of HER2. The morphological and structural attributes of the synthesized Pd nanostructures were thoroughly investigated using scanning electron microscopy, X-ray diffraction, X-ray photoelectron spectroscopy, and atomic force microscopy techniques. In-depth electrochemical investigations revealed an intimate correlation between the nanostructured sensor and electrochemical response, suggesting the suitability of hierarchical palladium nanostructures supported onto carbon nanotubes [Pd(−0.1 V)/CNT] for sensitive detection of HER2. The high surface area of hierarchical Pd nanostructures enabled an ultrasensitive electrochemical response toward HER2 (detection limit: 1 ng/mL) with a wide detection range of 10 to 100 ng/mL. The ease of surface modification, sensitivity, and reliable electrochemical response in human plasma samples suggested the enormous potential of Pd nanostructuring for chip-level point-of-care screening of HER2-positive breast cancer patients.

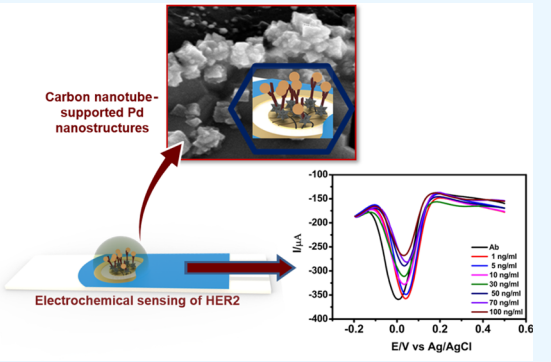

1. INTRODUCTION

The prevalence of breast cancer has witnessed a significant spike, with 2.2 million new cases every year.[1] Although curable when diagnosed early, 627,000 deaths in 2018 impose a substantial challenge to breast cancer diagnostics.[2] Though predictive tumor biomarkers (ER/PR/HER2) have facilitated the treatment, the overexpression of HER2 on breast epithelium indicates aggressive cell growth, poor prognosis, and shorter disease-free survival.[3,4] Although being observed in 30% of breast cancer patients, the condition needs to be considered seriously to reduce the mortality rate and guide HER2-positive breast cancer treatment.[5] The existing well-established diagnostics enzyme-linked immunoassay,[6] immunohistochemistry,[7] chromogenic in situ hybridization,[8] and fluorescence in situ hybridization,[9] are associated with false positives and poor patient compliance, suggesting the need for precision health care for efficient management of breast cancer.

Electrochemical biosensing technologies have rapidly expanded their potential for decentralized point-of-care breast cancer diagnostics in recent years. The primary emphasis remains to reach clinical standards in real sample matrices. Therefore, novel biosensing assays have continuously evolved through efficient integration of metal nanostructures (Au,[10] Ag,[11] Rh,[12] platinum,[13] and Cu nanoparticles (NPs)/nanoclusters),[14] carbon nanostructures,[15,16] metal oxides (MoO_3,[17] WO_3,[18] and Fe_3O_4[19]), molecularly imprinted polymers,[20] and quantum dots[21] to serve as immobilization matrices, signal amplifiers, labels, and peroxidase mimic for the detection process. In this regard, Yola et al. explored composites of gold NPs with copper-containing metal−organic frameworks (Cu-MOFs) and Cu_2ZnSnS_4 NPs/Pt/g-C_3N_4 for fabricating a sandwich-type nanostructured sensing interface for HER2 detection in serum samples from humans.[14] Further, Nasrollahpour et al. highlighted the application of biopolymer films generated through electrochemical deposition of WO_3/polyglutamic acid on glassy carbon electrode surfaces for reliable detection of HER2.[18] The proposed enzyme-free sensor demonstrated a significant electrochemical response toward HER2 with a detection limit (DL) of 1 fg/mL and a

Received: June 6, 2022
Accepted: August 30, 2022
Published: September 13, 2022

detection range of 1 ng/mL to 1 fg/mL. In another report, transition metal oxides like MoO_3 were anchored onto r-GO (reduced graphene oxide) to ensure a broad range detection of HER2 (1−500 ng/mL).[17] The significant electrochemical response was attributed to the enormously high surface area of MoO_3, excellent binding efficiency, and facile heterogeneous electron transfer (HET) to facilitate the detection of HER2.

Further, gold NP-modified antibody fragments of variable single chains were immobilized on disposable screen-printed electrodes to attain a dynamic detection range of 0.01−100 ng/mL toward HER2.[22] Likewise, laser-scribed graphene decorated with hierarchical gold nanostructures emerged as a potential immobilization matrix for performing ultra-sensitive point-of-care aptasensing of HER2 in clinical samples.[23] The unique Christmas tree-like appearance of gold nanostructures facilitated the immobilization of HER2-specific aptamers on the sensing interface for ultra-sensitive HER2 detection (DL: 0.008 ng/mL) in undiluted serum samples. Moreover, the laser-scribed graphene-based engineering approach was further implemented using a cell-phone-enabled electrochemical system to suggest its point-of-care clinical applications. Additionally, the concern has been recently widened toward tackling the biofouling of sensing interfaces through introducing polymers,[20] zwitterionic materials,[24] peptides,[25] and peptide hydrogels,[26] at the sensing electrode surface. Although effective, the major constituent of antifouling surfaces comprising polyethylene glycol and oligoethylene glycols are prone to poor water solubility and oxidative damage.[27] Moreover, the presence of hydrophobic layers on the electrode surfaces often limits the density and alignment of the recognition elements due to agglomeration and irregular distribution of the recognition elements on the electrode surface, demanding a sensitive and reproducible electrochemical response.[28]

Despite the growing emphasis on attaining clinically relevant electrochemical responses, the existing breast cancer diagnostics still suffer from significant bottlenecks restricting their commercial utilization. Primarily, interfacial probe density remains the major factor affecting electrochemical performance and mass reproducibility, along with minimal sample processing and consumption requirements.[29] In this regard, in situ growth of metal nanostructure arrays on the sensing electrodes has opened enormous possibilities for attaining tunable electrochemical response through effective size/shape modulation in a reproducible way.[30]

Palladium (Pd) and its composites have been used as labels and signal amplifiers for diverse immunosensing applications,[31−33] attributed to their exceptional physicochemical properties, strong electrocatalytic activity, and inherent affinity toward thiols and amines.[34] Considering the enormous potential, Pd nanostructures have been conveniently integrated to perform sensitive detection of HER2.[13,35] Recently, an ultrathin layer of Pd NPs was conjugated with HER2-specific peptides on a plastic substrate to develop a flexible sensing interface for the detection of HER2.[36] However, a reproducible, convenient, one-step, efficient manipulation of three dimensional (3-D) Pd nanostructures to attain maximal electrochemical response toward HER2 has not been implemented.

Therefore, in this work, we employed a one-step electroreduction method to develop hierarchical 3-D Pd nanostructures supported by carbon nanotubes (CNTs) for electrochemical sensing of HER2. After detailed morphological modulation at the axes of the potential/time/supporting electrolyte ratio with the palladium precursor, the proposed nanostructures were developed to ensure a reliable and sensitive electrochemical response toward HER2 detection.

Corresponding to the potential variations, hierarchical flower-like nanoclusters of Pd uniformly supported onto CNTs demonstrated superior electrochemical response toward detection of HER2. The sensor showed a significant ultra-low DL (1 ng/mL) toward HER2 over a wide detection range (10 to 100 ng/mL). The significant electrochemical response elucidated the morphological relevance of Pd nanostructures, facilitating reliable and efficient immobilization of antibodies specific to HER2 (anti-HER2) on the sensor surface. Further, excellent specificity against common interferents [IL6, IgG, and human serum albumin (HSA)] facilitated electrochemical detection of HER2 in human plasma samples. Moreover, the convenience and reproducibility of the proposed surface engineering approach extended its potential for developing robust, sensitive metallic nanostructured point-of-care devices for diverse immunosensing applications.

2. EXPERIMENTAL SECTION

2.1. Chemicals and Materials. Palladium chloride ($PdCl_2$), bovine serum albumin (BSA), potassium hexacyanoferrate(II)trihydrate [$K_4Fe(CN)_6{\cdot}3H_2O$], potassium hexacyanoferrate(III) [$K_3Fe(CN)_6$], EDC [1-ethyl-3-(3-dimethylaminopropyl)carbodiimide], *N*-hydroxysuccinimide (NHS), HSA, IL6, IgG, and oxidized CNTs (99.99% pure) were procured from Sigma-Aldrich. Sulfuric acid (H_2SO_4), hydrochloric acid (HCl), potassium chloride (KCl), potassium dihydrogen phosphate (KH_2PO_4), dipotassium hydrogen phosphate (K_2HPO_4), and sodium chloride (NaCl) were obtained from Merck. The plasma sample from a healthy subject was obtained as per the ethical committee approval number TEM-01/SOP-03-v05 dated 14th December 2021 and the institutional ethical committee approval from IISc (07/3.12.2021).

2.2. Electrochemical Synthesis of Pd-Nanostructured Electrodes. One mg of oxidized CNTs was ultrasonicated for 30 min in 1 mL of distilled water (conductivity > 10 MΩ cm^{-1}) for uniform dispersion. 20 μL of the as-prepared dispersion was drop-casted onto screen-printed gold electrodes. Hierarchical Pd nanostructures were uniformly grown over CNT-modified screen-printed electrodes using a convenient one-step electroreduction method using a Pd precursor ($PdCl_2$, 1 mM) and sulfuric acid (H_2SO_4, 0.01 M) at a constant potential (−0.1 V vs Ag/AgCl). Subsequently, the electrodeposited Pd nanostructures were morphologically evolved at the axes of potential and variable sulfuric acid/Pd precursors for investigating the morphology-induced electrochemical response toward HER2 detection.

2.3. Biofunctionalization of Pd-Nanostructured Electrodes. The immobilization process of anti-HER2 on cluster-like Pd nanostructures was adopted from previously reported literature.[37] Briefly, EDC (0.4 M), and NHS (0.1 M) in an equal amount of 100 μL were reacted with anti-HER2 (anti-HER2/EDC/NHS) in a 4:1:1 ratio to activate carboxyl groups of anti-HER2 for 30 min. After sufficient incubation, 20 μL of activated antibodies were drop-casted onto Pd-nanostructured screen-printed electrodes at 4 °C overnight. Further, the anti-HER2 immobilized electrodes were gently washed using 10 mM phosphate-buffered saline (PBS) (pH: 7.0) to remove untreated anti-HER2 from the screen-printed electrode

https://doi.org/10.1021/acsomega.2c03532
ACS Omega 2022, 7, 34177−34189

Scheme 1. Schematics Showing Different Steps Associated with the Fabrication of Pd(−0.1 V)/CNT-Based Immunosensor for HER2 Detection

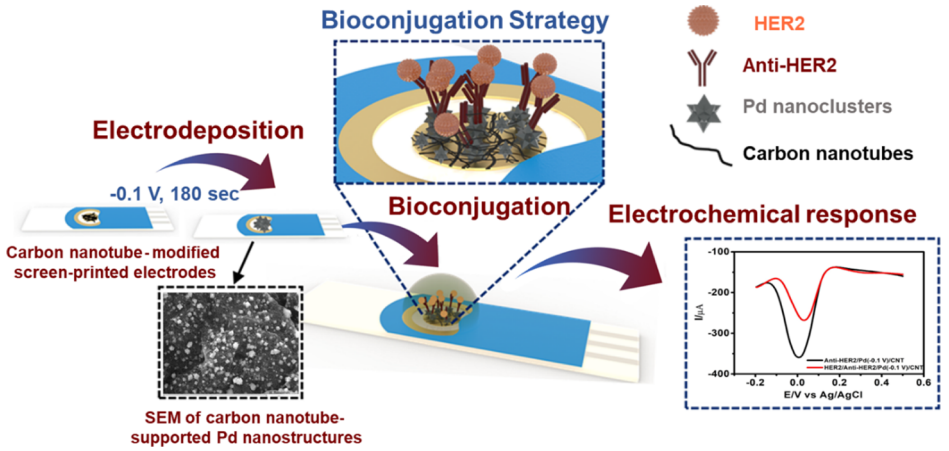

surfaces. The anti-HER2-immobilized CNT-supported Pd nanostructure [anti-HER2/Pd(−0.1 V)/CNT]-modified screen-printed electrode surfaces were incubated with 0.1 wt % BSA to avoid nonspecific binding during HER2 detection (Scheme 1). The fabricated [BSA/anti-HER2/Pd(−0.1 V)/CNT] immunoelectrodes were kept in the refrigerator (4 °C) for storage.

2.4. Characterization of the Pd-Nanostructured Electrodes. Detailed morphology analysis of the palladium nanostructures electrodeposited on the CNTs was executed using field-emission scanning electron microscopy (FE-SEM, JEOL JSM 7100F). The elemental composition of the nanostructures was analyzed using energy dispersive X-ray analysis (EDAX) through the in-built INCA Software, JEOL JSM 7100. The structural attributes of the deposited Pd nanostructures were confirmed using thin-film X-ray diffraction (XRD) patterns acquired from the Rigaku SmartLab X-ray diffractometer [Cu Kα radiation (1.5418 Å)]. The conjugation of anti-HER2 on the Pd-nanostructured surface was confirmed through Fourier transform infrared spectroscopy (FT-IR) within a wavelength range of 650−4000 cm^{-1} (PerkinElmer, Frontier). Detailed surface topographical changes associated with bioconjugation processes were analyzed using atomic force microscopy (AFM) from Park Systems NX-10. The different modification processes involved in the fabrication process of Pd(−0.1 V)/CNT-based immunosensors were imaged in the noncontact mode using silicon cantilevers under ambient conditions. Park Systems' software XEI_4.3.4 was used for data capture and image processing. The continuously evolving chemical environment corresponding to variable surface functionalization steps was probed in-depth using X-ray photoelectron spectroscopy (XPS) [Thermo Scientific, Kα (Al)]. The operation conditions included analysis chamber pressure: 10^{-9} mbar, loadlock chamber pressure: 10^{-9} mbar, and abode: Al Kα.

2.5. Electrochemical Characterization. Commercial chips (250 AT) from Metrohm with a three-electrode setup, including working electrode (Au, diameter 4 mm), counter electrode (Pt), and reference electrode (Ag), were modified for the fabrication of HER2 specific immunosensor. A pseudo reference electrode (Ag/AgCl) was electrochemically developed by applying a constant potential (1 V) for 10 s in a KCl solution with HCl (1 M, 50 μL) (Figure S1a in the Supporting Information). A potential difference of 70 mV was observed after the Ag/AgCl reference electrode formation (Figure S1b,c in the Supporting Information).

The electroanalytical techniques [cyclic voltammetry (CV), differential pulse voltammetry (DPV), and electrochemical impedance spectroscopy (EIS)] explored throughout this work were performed using a CH Instruments (model no. 660C) setup interfaced to a computer-controlled CH software package. The preliminary electrochemical analysis corresponding to the immobilization of anti-HER2 was performed using CV at a scan rate of 20 mV/s. The CV analysis studied the redox reaction of 5 mM $[Fe(CN)_6]^{3-}/[Fe(CN)_6]^{4-}$ in 10 mM PBS (pH 7.0) within the potential range of −0.2 to 0.4 V. Further, the charge transfer resistance's changes corresponding to the modification processes were evaluated using EIS at a constant potential of 0.2 V. The frequency range of 0.1 to 10^5 Hz was chosen for the analysis. The variable concentrations of HER2 were electrochemically analyzed using DPV (potential range: 0.5 to −0.3 V). All measurements were referenced using Ag/AgCl reference electrodes.

3. RESULTS AND DISCUSSION

3.1. Electrochemical Synthesis of Pd(−0.1 V)/CNT Electrodes. The general characteristics of the Pd electrodeposition were investigated on gold screen printed electrodes (250 AT, Metrohm) using CV analysis in 1 mM $PdCl_2$ solution and 0.01 M sulfuric acid as supporting electrolyte. While scanning from 0.8 to −0.6 V, the presence of a strong reductive peak (ca. 50 mV) indicates the conversion of Pd(II) to Pd(0), whereas a broadened oxidation peak (ca. 350 mV) corresponds well to the Pd metal adatoms oxidation[38] at the screen-printed gold electrode surfaces (Figure S2 in the Supporting Information).

Therefore, the electroreduction process of Pd was fine-tuned to gain control over the nucleation and growth of Pd nuclei for the development of morphologically tuned palladium nanostructures supported onto CNTs. The electrodeposition process employed the standard electroplating method suggesting a strong correlation between the deposition potential (0 V/−0.1 V/−0.2 V), reagent concentration, and supporting electrolyte on the morphology of the nanostructures.[39,40]

A controlled potential chronoamperometric technique was employed to study the impact of variable deposition potentials on the morphology of the Pd nanostructures. We observed a strong potential dependent morphological transformation of

https://doi.org/10.1021/acsomega.2c03532
ACS Omega 2022, 7, 34177−34189

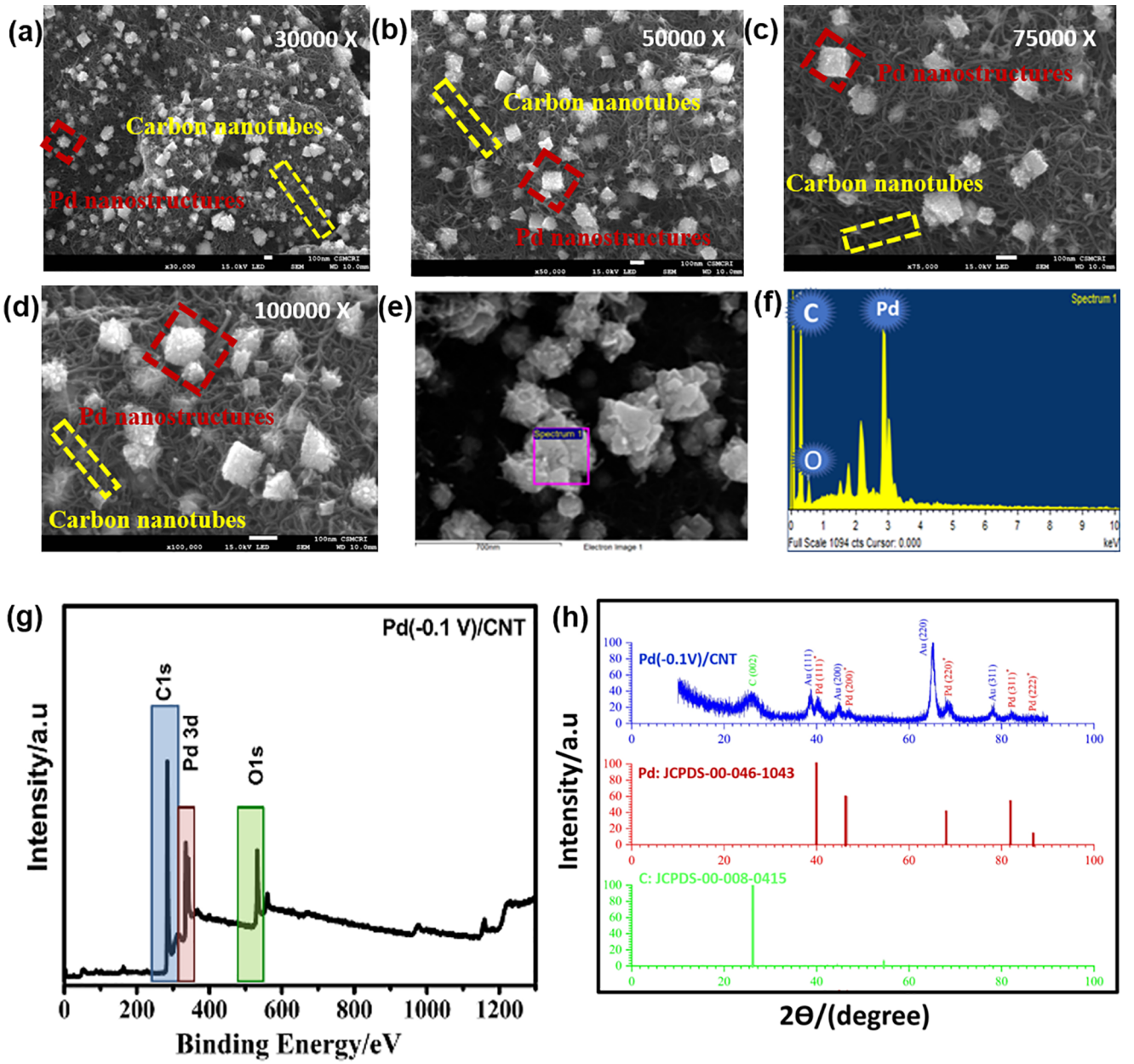

Figure 1. SEM images of hierarchical Pd nanostructures supported onto CNTs [Pd(−0.1 V)/CNT] at (a) 30,000×, (b) 50,000×, (c) 75,000×, and (d) 100,000×; (e) high resolution images of individual Pd nanostructures; (f) EDAX mapping of constituent elements in Pd(−0.1 V)/CNT; (g) X-ray survey scan spectra of Pd(−0.1 V)/CNT; and (h) XRD patterns of Pd(−0.1 V)/CNT with the standard JCPDS database.

Pd nanostructures on the CNT-modified screen-printed electrodes. Pd nanostructures demonstrated spherical, hierarchical cubical clusters and dense spheroids-like morphology under chosen potentials, respectively (Figure S3a,c,e in the Supporting Information). The variable morphology obtained was consistent with the accelerated kinetics of Pd nanostructuring at higher deposition potential values.[33] The optimized deposition potential was ensured after comparative cyclovoltammetric investigations {5 mM $[Fe(CN)_6]^{3-}$/$[Fe(CN)_6]^{4-}$ in 10 mM PBS (pH: 7.0)} to access an efficient immobilization of anti-HER2 followed by HER2 detection on variable Pd-nanostructured surfaces. The preliminary cyclovoltammetric analysis suggested a pronounced electrochemical response in the presence of HER2 (50 ng/mL) at Pd-nanostructured surfaces grown at the deposition potential of −0.1 V [Pd(−0.1 V)/CNT] (Figure S3b,d,f in the Supporting Information).

Considering an optimized electroreduction potential of −0.1 V, the impact of other driving parameters (Pd precursor and supporting electrolyte concentration) was evaluated for the significant morphological transformations to facilitate HER2 detection. The supporting electrolyte/Pd precursor ratios were further varied (5/10/50), and the impact of an increasing sulfuric acid concentration was observed on the growth of Pd(−0.1 V)/CNT. Although we observed no significant morphological transformation (Figure S4a,c,e in the Supporting Information), a consistently prominent electrochemical response was evident for Pd(−0.1 V)/CNT [supporting electrolyte/Pd ratio (10:1)] toward HER2 detection (Figure S4b,d,f in the Supporting Information). Therefore, Pd(−0.1 V)/CNT (electrodeposition conditions: −0.1 V; sulfuric/Pd:

https://doi.org/10.1021/acsomega.2c03532
ACS Omega 2022, 7, 34177−34189

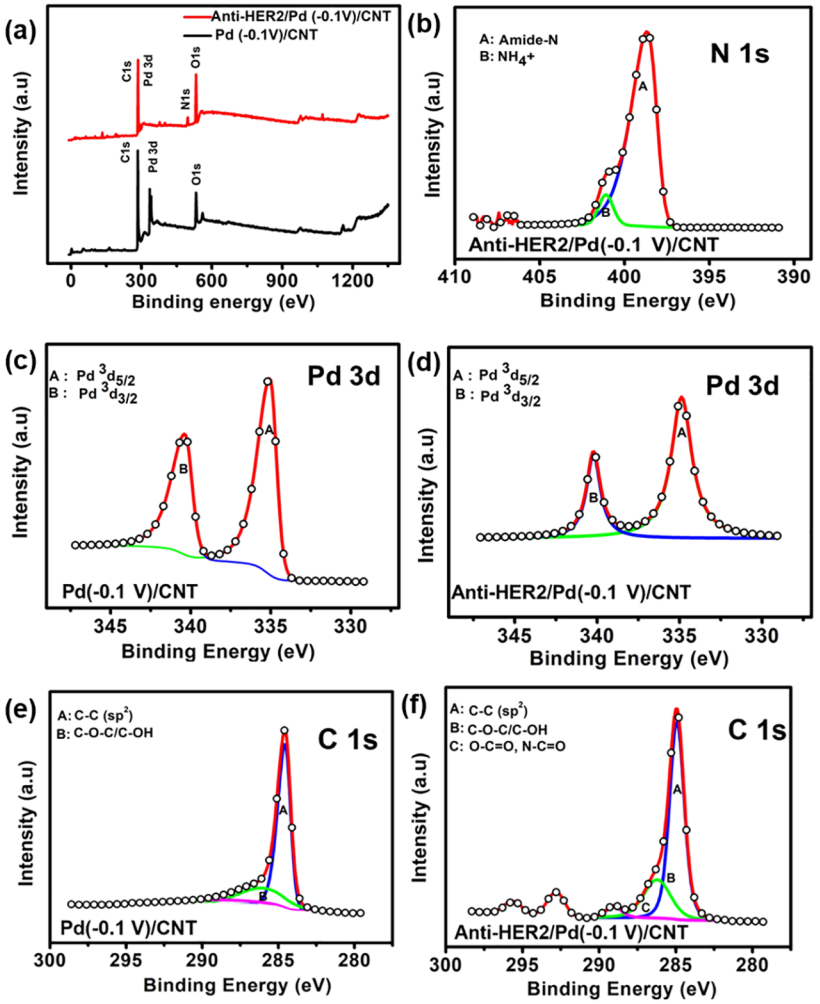

Figure 2. (a) Comparative X-ray survey scan spectra of Pd(−0.1 V)/CNT and anti-HER2/Pd(−0.1 V)/CNT, (b) N 1s core level spectra in anti-HER2/Pd(−0.1 V)/CNT-modified screen-printed electrodes, (c) Pd 3d core level spectra of Pd(−0.1 V)/CNT-modified screen-printed electrodes, (d) Pd 3d core level spectra of anti-HER2/Pd(−0.1 V)/CNT-modified screen-printed electrodes, (e) C 1s core level spectra of Pd(−0.1 V)/CNT-modified screen-printed electrodes, and (f) C 1s core level spectra of anti-HER2/Pd(−0.1 V)/CNT-modified screen-printed electrodes.

10/1, duration: 3 min) were further investigated for electrochemical sensing of the HER2 biomarker in detail.

FE-SEM images confirmed a uniform electrochemical deposition of Pd nanoclusters over tubular CNTs with sizes ranging from 99 to 122 nm (Figure S4c in the Supporting Information). A close morphological analysis under variable magnifications revealed hierarchical flower-like morphology of the Pd nanostructures on the tubular CNT network (Figure 1a−d). The hierarchical morphology is expected due to oxidative etching-induced twinned ridges in cube-shaped Pd nanostructures, which eventually diverge to give a flower-like appearance.[41] The uniform deposition of the Pd nanoclusters is most likely due to carboxyl moieties within the oxidized CNTs. The carboxyl functionalities served as anchoring sites for the Pd nuclei to nucleate and grow under the application of an electrodeposition potential (−0.1 V) for 180 s.

EDAX spectroscopy-based elemental analysis revealed strong peaks of Pd, O, and C elements with an atomic percentage of 45.18, 32.23, and 22.59%, respectively (Figure 1e,f). The EDAX observations were in close correlation with the XPS survey scan spectra obtained, confirming the presence of C 1s (284.5 eV), O 1s (529.6 eV), and Pd (335.1 eV) at corresponding binding energies (Figure 1g). The XPS spectra were plotted according to the C 1s peak at 284.5 eV. XRD-based structural analysis of the Pd(−0.1 V)/CNT revealed intense peaks at 2θ = 40.12, 46.66, 68.12, 82.10, and 86.62° assigned to the (111), (200), (220), (311), and (222) reflections of Pd (fcc lattice), respectively. The X-ray diffractogram was compared with the standard JCPDS database (Pd: JCPDS 00-046-1043). The comparative analysis confirmed the presence of cubical Pd nanostructures with space group $Fm\bar{3}m$ (225). An additional peak at 2θ = 26.43° was observed, corresponding to the characteristic (002) reflections from the CNTs. However, reflection (101) at 44.46° is partially obscured due to Pd's (200) plane. The obtained reflections were according to the 00-008-0415 database for hexagonal carbon (C) [space group $P6_3/mmc$ (194)] (Figure 1h).

We also observed prominent reflections (1 1 1), (2 0 1), (2 2 1), and (3 1 1) at diffraction angles 2θ = 38.19, 44.39, 64.58, and 77.55° from Au electrodes.

3.2. Fabrication of Pd(−0.1 V)/CNT Immunoelectrodes. The optimized electrochemical synthesis of hierarchical Pd nanostructures was further accompanied by the immobi-

https://doi.org/10.1021/acsomega.2c03532
ACS Omega 2022, 7, 34177−34189

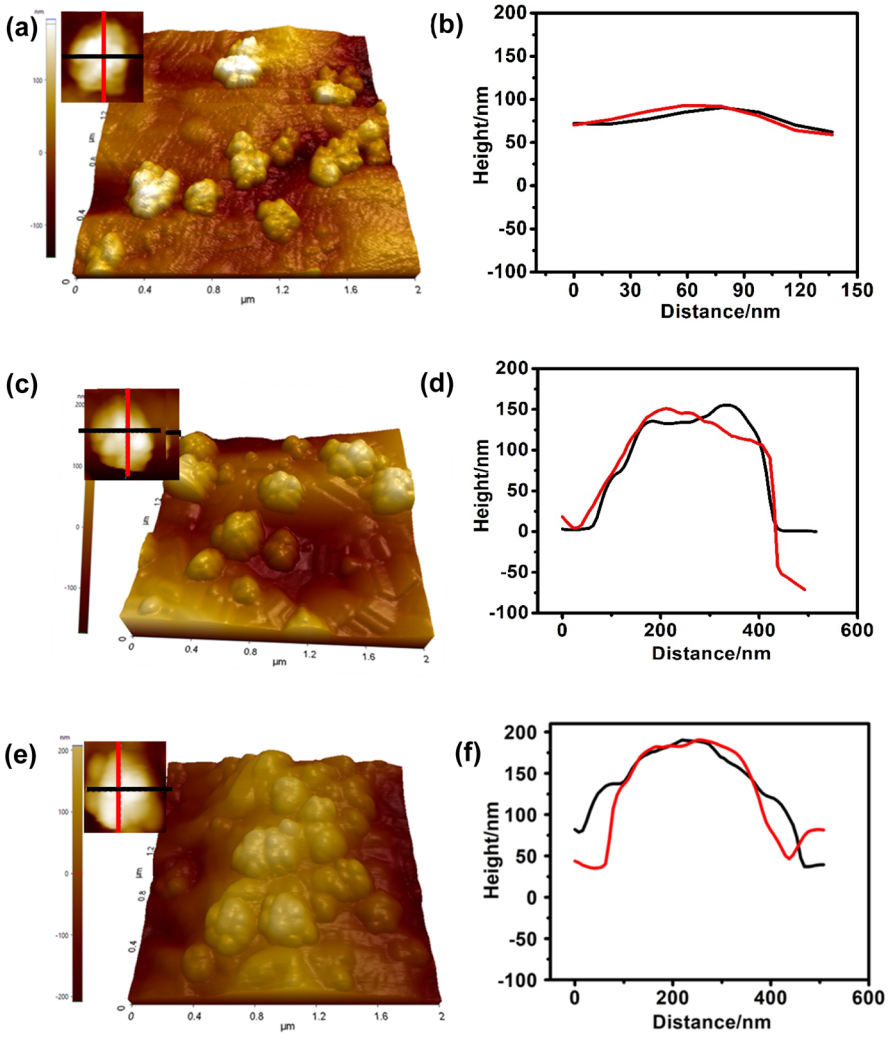

Figure 3. AFM analysis of (a) Pd(−0.1 V)-, (c) anti-HER2/Pd(−0.1 V)-, and (e) HER2/anti-HER2/Pd(−0.1 V)-modified screen-printed electrode surfaces. Corresponding cross sections analysis for (b) Pd(−0.1 V)-, (d) anti-HER2/Pd(−0.1 V)-, and (f) HER2/anti-HER2/Pd(−0.1 V)-modified screen-printed electrode surfaces.

lization of HER2-specific antibodies (anti-HER2) for HER2 detection. As specified in the Experimental Section, EDC/NHS mediated carbodiimide chemistry was employed to fabricate a Pd-nanostructured immunosensor. The detailed fabrication process of the anti-HER2/Pd(−0.1 V)/CNT immunosensor was characterized using FT-IR spectroscopy, XPS, AFM, and electrochemical techniques.

We conducted a detailed FT-IR spectroscopy-based functional group analysis to investigate the stepwise fabrication of the Pd-nanostructured immunosensor and its corresponding interaction with the target HER2 biomarker (Figure S5 in the Supporting Information). The successful modification of the screen-printed electrodes with Pd nanostructures supported onto CNTs demonstrated characteristic vibrations bands at 1511, 1725, and 1227 cm^{-1} due to the presence of the −C═C, −C═O, and −C−O functional groups, respectively, from the oxidized CNTs.[42] However, characteristic amide-I stretching (1630 cm^{-1}) and amide-II band (1565 cm^{-1}) correspond well to the C═O stretching of the peptide backbone and bending N−H modes of immobilized anti-HER2 on the Pd-nanostructured surface.[43,44] Further, the presence of the target HER2 biomarker showed an increase in the amide-II bands at 1565 cm^{-1} with a concomitant broadened −NH vibration peak centered at 3315 cm^{-1}. The observations confirmed the successful fabrication of the Pd-nanostructured immunosensor and its response toward HER2 detection.[45]

The preliminary FT-IR results were further supported with XPS investigations. Comparative survey scan spectra provided in Figure 2a revealed the presence of N 1s arising from the peptide bonds in the immobilized antibodies at anti-HER2/Pd(−0.1 V)/CNT electrode surfaces. The successful immobilization of anti-HER2 was further investigated by probing the changes in the chemical environment of C 1s, N 1s, O 1s, and Pd 3d after the modification process. The high-resolution N 1s core-level spectra confirmed the presence of amide-N linkage (NH−C═O) at 398.5 eV associated with the proteinaceous nature of anti-HER2.[46,47] The presence of an additional peak at 401.1 eV suggested the probability of ammonium (NH_4^+) species in lysine residues of the immobilized anti-HER2 (Figure 2b).[48]

The Pd 3d XPS spectra of Pd(−0.1 V)/CNT electrodes revealed two peaks (centered at 340.4 and 335.1 eV) associated with the binding energies of Pd $3d_{3/2}$ and Pd $3d_{5/2}$ components. The spin−orbital splitting at 5.3 eV further confirmed the metallic state of Pd (Pd^0) in Pd(−0.1 V)/CNT (Figure 2c).[49] However, anti-HER2/Pd(−0.1 V)/CNT

https://doi.org/10.1021/acsomega.2c03532
ACS Omega 2022, 7, 34177−34189

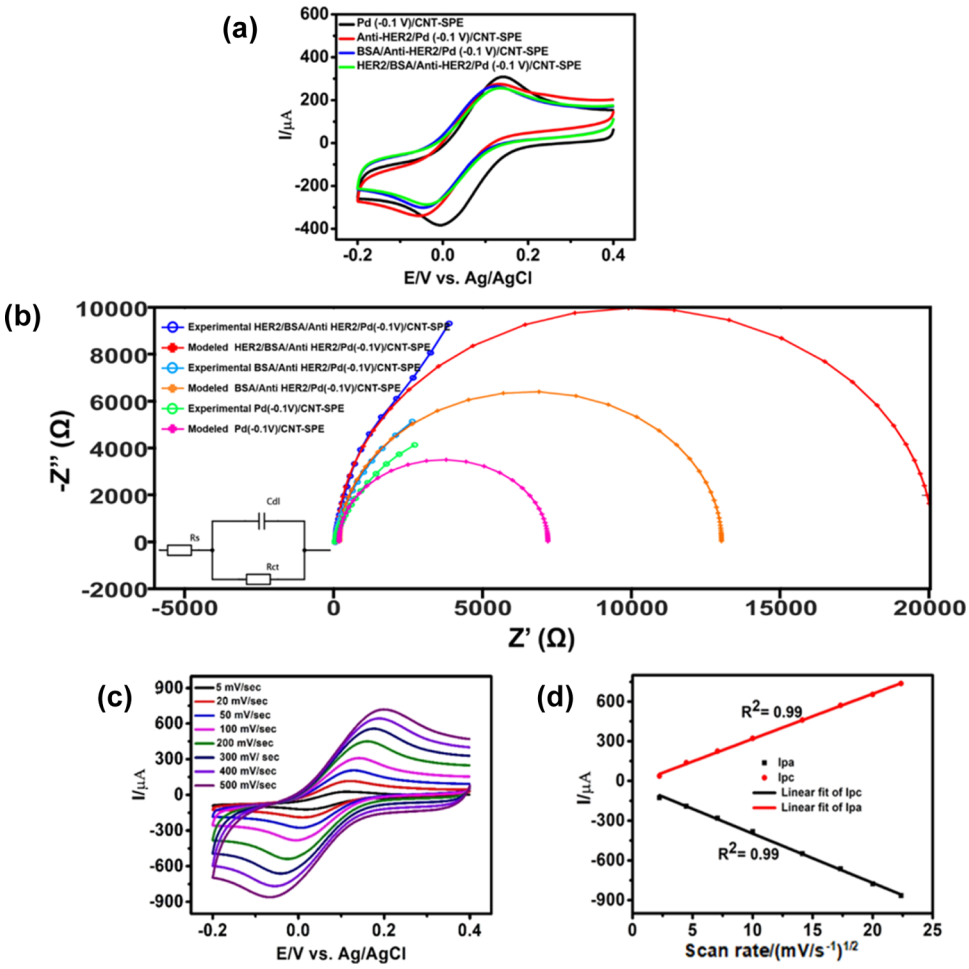

Figure 4. (a) Cyclic voltammograms of different Pd(−0.1 V)/CNT-modified electrodes surfaces in 5 mM $[Fe(CN)_6]^{3-/4-}$at a scan rate of 20 mV/s, (b) electrochemical impedance spectroscopic analysis of different Pd(−0.1 V)/CNT-modified electrode surfaces in 5 mM $[Fe(CN)_6]^{3-/4-}$ in 10 mM PBS (pH 7.0) at a potential value of 0.2 V, (c) electrochemical response of Pd(−0.1 V)/CNT-modified screen-printed electrode surface at variable scan rates ranging from 5 to 500 mV/s, and (d) corresponding linear relation of current response with the scan rate ($v^{1/2}$) in accordance to the diffusion-controlled electrochemical response.

electrodes demonstrated no significant shift in binding energies associated with Pd $3d_{5/2}$ and Pd $3d_{3/2}$ components suggesting that Pd nanostructures are loosely bound to the anti-HER2 without any probability of charge transfer (Figure 2d).[50] We observed a significant reduction in the intensity of Pd $3d_{5/2}$ and Pd $3d_{3/2}$ components as a consequence of supramolecular assembly of the anti-HER2 layers on the anti-HER2/Pd(−0.1 V)/CNT electrodes (Figure S6 in the Supporting Information).[51]

The deconvolution of C 1s core-level spectra confirmed different C species [C−C(sp^2)(284.5 eV), C−O−C/C−OH (285.9 eV)] in Pd(−0.1 V)/CNT electrode surfaces (Figure 2e).[52−54] However, a significant shift in the C−OH binding energies and characteristic N−C═O bonds (289.3 eV) confirms the successful immobilization of anti-HER2 on Pd(−0.1 V)/CNT electrode surfaces (Figure 2f).[48] Moreover, oxygen species in both the modified electrodes confirm the presence of carboxylic functional groups (OH−C═O) attributed to the oxidized CNTs (as a supporting matrix) on the screen-printed electrodes (Figure S7 in the Supporting Information).

The noncontact mode of the atomic force microscope was employed to confirm the successful fabrication of the HER2 immunosensor. The topographical changes arising from Pd nanostructures facilitated immobilization of anti-HER2, and corresponding anti-HER2 and HER2 interactions are shown in Figure 3a,c,e. The root mean square value extracted from topographic AFM images indicates the change in roughness values after each modification process. Corresponding cross-sections of the 3-D AFM images are provided as insets of Figure 3a,c,e. The bare screen-printed Au electrode exhibited a surface roughness of 27 nm (Figure S8a in the Supporting Information), which observed a significant increase (45 nm) after uniform electrochemical deposition of Pd nanostructures (Figure 3a). The uniform deposition of Pd nanostructures was evident from the fast Fourier transform image analysis of the Pd(−0.1 V)-modified electrode surfaces (Figure S9 in the Supporting Information). Cross-section-based height profile analysis suggested an 80−100 nm size for the electrodeposited Pd nanoclusters (Figure 3b).

The carbodiimide-mediated immobilization of the antibodies (1 μg/mL) leads to a significant increase in the surface roughness (64 nm) due to isotopically distributed "islands" of Pd nanostructures uniformly covered with anti-HER2 (Figure 3c). The obtained results were consistent with SEM images of the anti-HER2/Pd(−0.1 V) nanostructured surface (Figure S8b in the Supporting Information). Cross-section analysis suggested that anti-HER2 modified Pd nanoclusters lie in the

https://doi.org/10.1021/acsomega.2c03532
ACS Omega 2022, 7, 34177−34189

size range of 140−150 nm (Figure 3d). The significant increase in surface roughness corresponding to anti-HER2 immobilization was consistent with existing reports.[55]

We further observed an increase in surface roughness (95 nm) corresponding to the interaction of anti-HER2 with target HER2 (100 ng/mL) on Pd-nanostructured surfaces (Figure 3e). Moreover, the cross-section of uniformly decorated clusters witnessed a further increase (175−200 nm) attributed to successful immunocomplex formation on the electrode surfaces (Figure 3f).

3.3. Electrochemical Characterization of Pd(−0.1 V)/CNT Immunoelectrodes. The sequential stepwise modification of the screen-printed electrodes [Pd(−0.1 V)/CNT; anti-HER2/Pd(−0.1 V)/CNT; BSA/anti-HER2/Pd(−0.1 V)/CNT; and HER2/BSA/anti-HER2/Pd(−0.1 V)/CNT] was comprehensively investigated using CV and EIS studies. As shown in Figure 4a, CV studies were carried out using 5 mM $[Fe(CN)_6]^{3-}/[Fe(CN)_6]^{4-}$ in 10 mM PBS (pH: 7.0; scan rate: 20 mV/s) at different modified electrodes surfaces. Preliminary CV investigations showed reversible redox peaks (E_{pa}: ca. 141 mV and E_{pc}: −5 mV) with enhanced currents (I_{pa}: 314.46 μA and I_{pc}: −388.21 μA) at Pd(−0.1 V)/CNT modified electrode surfaces. The electrochemical response obtained at the Pd(−0.1 V)/CNT electrode surface signifies a synergistic combination of Pd nanostructures and CNTs for facile electron transfer at the electrode surfaces.[56,57] The concept of the synergistic combination was experimentally investigated in detail through comparative morphological analysis for both Pd(−0.1 V)/SPE and Pd(−0.1 V)/CNT/SPE surfaces.

We observed sparsely distributed spherical Pd nanoclusters (82−150 nm) on the bare screen-printed electrode surfaces, which further transformed to dense, oriented, and high surface area hierarchical Pd nanostructures after modification with oxidized CNTs on screen-printed electrodes (Figure S10a,b in the Supporting Information). The presence of carboxyl moieties on the CNTs is supposed to facilitate nucleation, followed by the growth of Pd nuclei into hierarchical Pd nanostructures on the CNT-modified screen-printed electrode surfaces. Compared with randomly distributed Pd nanostructures [Pd(−0.1 V)/SPE], the dense coverage of the screen-printed electrodes with the CNTs supported hierarchical Pd nanostructures [Pd(−0.1 V)/CNT/SPE] is likely to improve the loading and orientation of anti-HER2 on the electrode surface for HER2 detection.

After modification with anti-HER2, the Pd(−0.1 V)/CNT electrodes demonstrated reduced electrochemical response with an oxidative and reductive peak current of 278.36 and −337.68 μA, respectively. The electrochemical response was attributed to the hindrance of $[Fe(CN)_6]^{3-}/[Fe(CN)_6]^{4-}$ mass transfer due to insulating macromolecular layers of anti-HER2,[58] confirming an efficient immobilization of anti-HER2 on the Pd-nanostructured electrode surfaces. After incubation with the HER2 biomarker (50 ng/mL), the electrochemical response was further suppressed due to anti-HER2−HER2 immunocomplexes on the electrode surfaces. The highly specific recognition event arising from van der Waals, hydrophobic, electrostatic, and hydrogen bonds are expected to develop a thin insulating layer, affecting the mobility of electrons at the Pd-nanostructured electrode surface.[59]

Detailed comparative CV analysis confirms the successful fabrication of the HER2 immunosensor with a sequential decrease in electrochemical response corresponding to each biomolecular immobilization process on the electrode surfaces in the following manner:

Pd(−0.1 V)/CNT > anti-HER2/Pd(−0.1 V)/CNT > BSA/anti-HER2/Pd(−0.1 V)/CNT > HER2/BSA/anti-HER2/Pd(−0.1 V)/CNT.

We further investigated the change in the diffusion coefficient (D) corresponding to each biomolecular immobilization process on the Pd(−0.1 V)/CNT modified electrode surfaces using the Randles−Sevcik equation[60]

$$I_p = 2.69 \times 10^5 n_2^3 ACD_2^1 \vartheta^{0.5} \quad (1)$$

where I_p = anodic peak current; n = number of electrons involved (1); A = geometric area of the screen-printed electrodes (0.12 cm^2); C = redox species's concentration (5 mM); and ϑ = scan rate (20 mV/s).

The Pd(−0.1 V)/CNT modified electrode surfaces exhibited a D value of 1.89×10^{-4} cm^2/s suggesting a facile e-transfer from the electrolyte. Further, modification with anti-HER2 and target HER2 biomarkers hinders the diffusion process at the electrode−electrolyte interfaces with a D value of 1.48×10^{-4} and 1.26×10^{-4} for anti-HER2/Pd(−0.1 V)/CNT- and HER2/BSA/anti-HER2/Pd(−0.1 V)/CNT-modified electrodes, respectively (Table S1 in the Supporting Information). The HET kinetics of different modified electrode surfaces was further investigated using EIS. As shown in Figure 4b, Nyquist plots were consistent with cyclovoltammetric analysis suggesting a sequentially increasing charge transfer resistance with each biomolecular immobilization process on the Pd(−0.1 V)/CNT surface.

The EIS data were fitted to Randle's circuit model involving resistance (charge transfer), resistance (solution), and double layer capacitance (C_{dl}). After fitting equivalent circuit elements, we observed a significant increase in charge transfer resistance with subsequent biomolecular immobilization processes on the Pd-nanostructured interfaces. The Pd-nanostructured interfaces exhibited an R_{ct} value of 8000 Ω, which increased to 10,000 Ω after successful immobilization of anti-HER2. The proteinaceous nature of the anti-HER2 creates an insulating layer to passivate the conducting electrode surface, which was consistent with the increased R_{ct} value. The highly specific recognition of the immobilized anti-HER2 with the target HER2 (50 ng/mL) further increased the R_{ct} value (20,000 Ω) due to immunocomplexes formation on the electrode surfaces.

The sequential increase in the charge transfer resistance in the following way confirms the successful fabrication of the Pd-nanostructured immunosensor for detecting HER2.

HER2/BSA/anti-HER2/Pd(−0.1 V)/CNT (20,000 Ω) > BSA/anti-HER2/Pd(−0.1 V)/CNT (10,000 Ω) > Pd(−0.1 V)/CNT (8000 Ω).

The lowest R_{ct} obtained for Pd(−0.1 V)/CNT was in accordance with the diffusion coefficient analysis emphasizing a facile electron transfer process at the Pd(−0.1 V)/CNT electrode surfaces. The uniformly deposited Pd nanostructures served as conduction pockets for facilitating charge transfer on CNTs.[61]

3.3.1. Scan Rate Studies. The kinetics of Pd(−0.1 V)/CNT electrode interfaces was investigated in detail at variable scan rates (5, 20, 50, 100, 200, 300, 400, and 500 mV/s) using 5 mM of the $[Fe(CN)_6]^{3-}/[Fe(CN)_6]^{4-}$ redox mediator. The cyclovoltammetric analysis revealed a continuous increase in peak current (anodic and cathodic components) (Figure 4c) with a concomitant positive shift in the oxidative peak

https://doi.org/10.1021/acsomega.2c03532
ACS Omega 2022, 7, 34177−34189

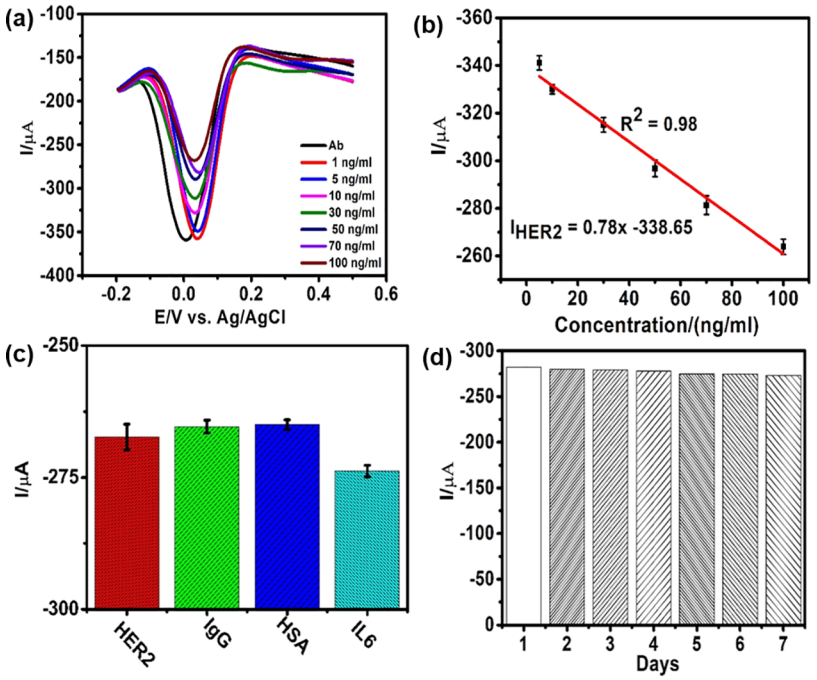

Figure 5. (a) Differential pulse voltammograms of BSA/anti-HER2/Pd(−0.1 V)/CNT immunoelectrodes in 5 mM $[Fe(CN)_6]^{3-/4-}$ at varying HER2 concentrations, (b) corresponding calibration plots suggesting linear relation of cathodic peak current (I) and concentration of HER2, (c) selectivity assay of BSA/anti-HER2/Pd(−0.1 V)/CNT immunosensor toward detection of HER2 in presence of interferences (IgG, HSA, and IL6), and (d) stability of electrochemical response of BSA/anti-HER2/Pd(−0.1 V)/CNT immunoelectrodes toward HER2 detection.

potential and a negative shift in the reduction peak potential with an increase in the scan rates (Table S2 in the Supporting Information). Moreover, increased peak−peak potential separation values (ΔE_p) at higher scan rates supported reversible electrode kinetics at Pd(−0.1 V)/CNT electrode surfaces (Figure S11 in the Supporting Information).[62]

The anodic and cathodic components of peak currents (I_{pa} and I_{pc}) linearly varied with the square root of scan rate ($\nu^{1/2}$) [regression coefficient (R^2 = 0.99)]. The observed electrochemical response was in close agreement with the diffusion-limited e-transfer processes suggested by the Randles−Sevcik equation (Figure 4d).[60] Therefore, diffusion-controlled e-transfer processes were dominant for the Pd-nanostructured electrodes based on the following equations

$$I_{pa} = 33.66x - 25.70 \quad R^2 = 0.99 \tag{2}$$

$$I_{pc} = -35.9x - 43.55 \quad R^2 = 0.99 \tag{3}$$

Several essential parameters were optimized to ensure a reliable and sensitive electrochemical response toward HER2 detection. The electrochemical response is significantly impacted due to the conformation of immobilized proteins and the pH of the supporting electrolyte. Considering the physiological conditions of human blood plasma and avoiding denaturation of HER2 and anti-HER2, pH 7.0 was considered throughout the electrochemical studies. The highly specific interaction of the antibodies with the target antigen remains crucial for the performance of the electrochemical immunosensor. Therefore, the interaction of anti-HER2 and HER2 was studied for variable time durations using the differential pulse voltammetric technique (DPV) in 5 mM $[Fe(CN)_6]^{3-}$/$[Fe(CN)_6]^{4-}$ in 10 mM PBS (Figure S12a in the Supporting Information). The cathodic peak current response decreased (−379.54 to −363.45 μA) with the increase in time duration (10−30 min) and further attained a steady-state after 30 min (Figure S12b in the Supporting Information). Therefore, an interaction time of 40 min at room temperature (25 °C) was chosen for all the electrochemical measurements. The nanostructured sensing surfaces are subjected to fouling due to nonspecific interactions. Therefore, the stability of the BSA/anti-HER2/Pd(−0.1 V)/CNT was ensured by performing repetitive cyclovoltammetric measurements in 5 mM $[Fe(CN)_6]^{3-}$/$[Fe(CN)_6]^{4-}$ for 50 cycles (Figure S12c in the Supporting Information). The electrochemical response was stable for 50 cycles with less than 5% current change.

The analytical response of BSA/anti-HER2/Pd(−0.1 V)/CNT-based electrochemical immunosensor was evaluated under variable concentrations of HER2 using the sensitive DPV technique. The BSA/anti-HER2/Pd(−0.1 V)/CNT-modified electrodes were incubated with varying concentrations of HER2 (1−100 ng/mL) for 40 min, and a corresponding DPV response was obtained using 5 mM $[Fe(CN)_6]^{3-}$/$[Fe(CN)_6]^{4-}$ in 10 mM PBS within a potential range of 0.6 to −0.2 V. As shown in Figure 5a, the cathodic component of peak current sequentially declined with a subsequent increase in HER2 concentration within a range of 1−100 ng/mL. The obtained electrochemical response indicates an incremental hindrance in the mass transfer of the $[Fe(CN)_6]^{3-}$/$[Fe(CN)_6]^{4-}$ corresponding to the formation of anti-HER2−HER2 immunocomplexes at variable concentrations of HER2.[50] Corresponding calibration curves (current vs concentration of HER2) provided as Figure 5b suggested a linear dependence within 10−100 ng/mL concentrations of HER2 with following linear regression equations.

$$I_{HER2} = 0.78C_{HER2} - 338.65 \quad R^2 = 0.98 \tag{4}$$

https://doi.org/10.1021/acsomega.2c03532
ACS Omega 2022, 7, 34177−34189

We have considered the limit of quantitation as the DL, as a visible change in the electrochemical response was observed in the presence of 1 ng/mL.[22] However, based on the standard DL formula, the sensor demonstrated a limit of detection (LOD) of 17.3 ng/mL.[63]

$$\mathrm{LOD} = (3.3 \times \sigma/S)$$

where σ = standard deviation of the linear response and S = slope of the calibration curve.

As compared with existing reports (electrodes, electrochemical methods, detection range, and DL) (Table S3 in the Supporting Information), the analytical response of the proposed Pd-nanostructured immunosensor was reproducible and sensitive with a low DL. The peak current change (ΔI) corresponding to the interaction of HER2 at variable concentrations is shown in Figure S13 in the Supporting Information. Moreover, it enabled a convenient approach for in situ modification for point-of-care devices.

3.4. Reproducibility, Specificity, and Stability of the HER2 Immunosensor. The reproducibility of the Pd-nanostructured immunosensor was evaluated at variable fabrication levels to ensure its clinical applications. The reliability of Pd nanostructuring on CNT-modified screen-printed electrodes was confirmed for three different electrodes. The chronoamperometric electrochemical response was identical for the studied three electrodes (Figure S14a in the Supporting Information). Further, the orientation of Pd nanostructures aligned antibodies was compared with well-established protein G chemistry. The comparable electrochemical response suggested site-specific orientation of anti-HER2 on the Pd(−0.1 V)/CNT electrode surfaces (Figure S14b in the Supporting Information). The electrochemical response of three identically fabricated BSA/anti-HER2/Pd(−0.1 V)/CNT modified electrodes was evaluated for HER2 detection using the DPV technique. The electrochemical response was consistent [relative standard deviation (RSD)] of 1.8% (Figure S14c in the Supporting Information) for the studied immunoelectrodes.

The response of the fabricated HER2 immunosensor was further assessed with other cancer-specific biomarkers present in the blood samples. Therefore, BSA/anti-HER2/Pd(−0.1 V)/CNT modified electrodes were incubated with 20 ng/mL of nonspecific biomarkers (IgG, IL6, and HSA) with 100 ng/mL of HER2 for 40 min. The DPV response demonstrated a highly specific response in the presence of IgG, IL6, and HSA with negligible change in the electrochemical signal (Figure 5c). An acceptable interference was observed with a less than 5% change in the electrochemical signal suggesting an excellent specificity against the studied interferents.

The stability of the electrochemical response was evaluated for seven days. The fabricated electrochemical immunosensor was stored for seven days (4 °C), and DPV response was measured each day after incubating 100 ng/mL HER2. The electrochemical activity of the sensor remained unchanged for seven days, suggesting a stable electrochemical response of the sensor over seven days (Figure 5d).

3.5. Real Sample Analysis. The potential suitability of the Pd-nanostructured immunoassay was evaluated for HER2 detection in human plasma samples. The plasma sample from a healthy individual was diluted 1000 times with PBS (10 mM pH: 7.0) and spiked with three known concentrations (5, 10, and 30 ng/mL). The comparable DPV response with a rational correlation in PBS (Figure S15 in the Supporting Information) was obtained with an RSD of 1.80, 0.6, and 2.28%, respectively (Table S4 in the Supporting Information). The peak currents corresponding to the HER2 concentrations added in the plasma samples were different ($p < 0.05$) when tested with the Student's t-test assuming unequal variance. The results suggested that the proposed Pd nanostructures-based assay has the potential to be implemented for HER2 detection from the plasma samples of breast cancer patients.

4. CONCLUSIONS

Hierarchical Pd nanostructures developed through a convenient one-step electroreduction method have been employed for label-free HER2 detection. The work highlighted the morphology-dependent electrochemical response of Pd-nanostructured immunosensor facilitated through an efficient coverage of anti-HER2 on the sensor surface. Detailed FT-IR, XPS, AFM, and electrochemical investigations suggested an efficient biofunctionalization on the Pd-nanostructured sensor surface. The excellent affinity of the hierarchical Pd nanostructures combined with high surface area CNTs enabled a dynamic detection range (10−100 ng/mL) with excellent sensitivity toward HER2 (DL: 1 ng/mL). The reproducible modification process, oriented alignment, and consistent electrochemical response supported the potential of the proposed immunoassay for point-of-care clinical settings. Furthermore, the specific response toward cointerferents in the blood (IgG, IL6, and HSA) facilitated its application for detecting HER2 in plasma samples. The sensor demonstrated an acceptable accuracy for HER2 detection in plasma samples to support its potential for future ultra-sensitive point-of-care immunosensing platforms. Moreover, the approach's convenience, robustness, and universal nature marked its potential for diverse immunosensing applications. We envisage exploring crosslinked peptides−metal nanostructure arrays as antifouling sensing interfaces for detecting cancer biomarkers in undiluted biological samples.

■ ASSOCIATED CONTENT

Supporting Information

The Supporting Information is available free of charge at https://pubs.acs.org/doi/10.1021/acsomega.2c03532.

Development of the Ag/AgCl reference electrode and its electrochemical response; CV response of palladium electrodeposition; FE-SEM images of different potential variants of Pd nanostructures; FE-SEM images of Pd nanostructures generated under variable Pd precursors and sulfuric acid ratios; stepwise FT-IR analysis of Pd(−0.1 V)/CNT immunoelectrodes; Pd 3d core level XPS spectra of variable Pd-nanostructured screen-printed electrodes; O 1s core-level XPS spectra of Pd-nanostructured screen-printed immunoelectrodes; topographical analysis of the bare Au screen-printed electrode and SEM image of Pd-nanostructured immunoelectrodes; fast Fourier transform images of variable modification processes; morphological analysis of Pd(−0.1 V)/SPE and Pd(−0.1 V)/CNT SPE; dependence of ΔE_p of Pd(−0.1 V)/CNT electrodes at variable scan rates; optimization studies associated with the fabrication of Pd-nanostructured immunosensor; calibration response of the HER2 immunosensor; reproducibility studies associated with the fabrication

https://doi.org/10.1021/acsomega.2c03532
ACS Omega 2022, 7, 34177−34189

process of the immunosensor; and real sample analysis (PDF)

AUTHOR INFORMATION

Corresponding Author

Hardik J. Pandya − *Department of Electronic Systems Engineering, Division of EECS, Indian Institute of Science, Bangalore 560012, India;* orcid.org/0000-0001-9835-8323; Email: hjpandya@iisc.ac.in

Authors

Anju Joshi − *Department of Electronic Systems Engineering, Division of EECS, Indian Institute of Science, Bangalore 560012, India*

Anil Vishnu G K − *Centre for BioSystems Science and Engineering, Indian Institute of Science, Bangalore 560012, India*

Dhananjay Dhruv − *Natubhai V. Patel College of Pure and Applied Sciences, Charutar Vidya Mandal University, Anand 388120 Gujarat, India*

Vishnu Kurpad − *SriShankara Cancer Hospital and Research Centre, Bengaluru 560004 Karnataka, India*

Complete contact information is available at: https://pubs.acs.org/10.1021/acsomega.2c03532

Notes

The authors declare no competing financial interest.

ACKNOWLEDGMENTS

The authors acknowledge Professor Navakanta Bhat, CENSE, IISc Bangalore, for providing access to the electrochemical workstation and lab facilities. A.J. acknowledges Ajay Krishnan for preparing Scheme [1]. H.J.P. acknowledges funding support under the Biomedical Device and Technology Development (BDTD) programme of the Department of Science and Technology (DST), Government of India (SP-DSTO-0019). A.V.G.K. acknowledges the award funding from the Biotechnology Industry Research Assistance Council (BIRAC) under the SITARE-Gandhian Young Technological Innovation Award (GYTI) scheme (BIRAC SRISTI PMU-2020/001). A.J. acknowledges the Science and Engineering Research Board, Government of India, for the National Postdoctoral Fellowship (PDF/2019/002621). The authors thank Dr. Manjula Das, Mazumdar Shaw Medical Centre, for her valuable feedback throughout the execution of this study.

REFERENCES

(1) Sung, H.; Ferlay, J.; Siegel, R. L.; Laversanne, M.; Soerjomataram, I.; Jemal, A.; Bray, F. Global Cancer Statistics 2020: GLOBOCAN Estimates of Incidence and Mortality Worldwide for 36 Cancers in 185 Countries. *Ca-Cancer J. Clin.* **2021**, *71*, 209−249.

(2) Rahman, S. A.; Al−Marzouki, A.; Otim, M.; Khalil Khayat, N. E. H. K.; Yousuf, R.; Rahman, P. Awareness about Breast Cancer and Breast Self-Examination among Female Students at the University of Sharjah: A Cross-Sectional Study. *Asian Pac. J. Cancer Prev.* **2019**, *20*, 1901−1908.

(3) Waks, A. G.; Winer, E. P. Breast Cancer Treatment: A Review. *J. Am. Med. Assoc.* **2019**, *321*, 288−300.

(4) Ahirwar, R. Recent Advances in Nanomaterials-Based Electrochemical Immunosensors and Aptasensors for HER2 Assessment in Breast Cancer. *Mikrochim. Acta* **2021**, *188*, 317.

(5) Shah, S.; Chen, B. Testing for HER2 in Breast Cancer: A Continuing Evolution. *Pathol. Res. Int.* **2010**, *2011*, 903202.

(6) Tian, S.; Zeng, K.; Yang, A.; Wang, Q.; Yang, M. A Copper Based Enzyme-Free Fluorescence ELISA for HER2 Detection. *J. Immunol. Methods* **2017**, *451*, 78−82.

(7) Zaha, D. C. Significance of Immunohistochemistry in Breast Cancer. *World J. Clin. Oncol.* **2014**, *5*, 382−392.

(8) Kiyose, S.; Igarashi, H.; Nagura, K.; Kamo, T.; Kawane, K.; Mori, H.; Ozawa, T.; Maeda, M.; Konno, K.; Hoshino, H.; Konno, H.; Ogura, H.; Shinmura, K.; Hattori, N.; Sugimura, H. Chromogenic in Situ Hybridization (CISH) to Detect HER2 Gene Amplification in Breast and Gastric Cancer: Comparison with Immunohistochemistry (IHC) and Fluorescence in Situ Hybridization (FISH). *Pathol. Int.* **2012**, *62*, 728−734.

(9) Mass, R. D.; Press, M. F.; Anderson, S.; Cobleigh, M. A.; Vogel, C. L.; Dybdal, N.; Leiberman, G.; Slamon, D. J. Evaluation of Clinical Outcomes According to HER2 Detection by Fluorescence In Situ Hybridization in Women with Metastatic Breast Cancer Treated with Trastuzumab. *Clin. Breast Cancer* **2005**, *6*, 240−246.

(10) Rostamabadi, P. F.; Heydari-Bafrooei, E. Impedimetric Aptasensing of the Breast Cancer Biomarker HER2 Using a Glassy Carbon Electrode Modified with Gold Nanoparticles in a Composite Consisting of Electrochemically Reduced Graphene Oxide and Single-Walled Carbon Nanotubes. *Microchim. Acta* **2019**, *186*, 495.

(11) Shamsipur, M.; Emami, M.; Farzin, L.; Saber, R. A Sandwich-Type Electrochemical Immunosensor Based on in Situ Silver Deposition for Determination of Serum Level of HER2 in Breast Cancer Patients. *Biosens. Bioelectron.* **2018**, *103*, 54−61.

(12) Sadeghi, M.; Kashanian, S.; Naghib, S. M.; Arkan, E. A High-Performance Electrochemical Aptasensor Based on Graphene-Decorated Rhodium Nanoparticles to Detect HER2-ECD Oncomarker in Liquid Biopsy. *Sci. Rep.* **2022**, *12*, 3299.

(13) Ou, D.; Sun, D.; Lin, X.; Liang, Z.; Zhong, Y.; Chen, Z. A Dual-Aptamer-Based Biosensor for Specific Detection of Breast Cancer Biomarker HER2 via Flower-like Nanozymes and DNA Nanostructures. *J. Mater. Chem. B* **2019**, *7*, 3661−3669.

(14) Yola, M. L. Sensitive Sandwich-Type Voltammetric Immunosensor for Breast Cancer Biomarker HER2 Detection Based on Gold Nanoparticles Decorated Cu-MOF and Cu2ZnSnS4 NPs/Pt/g-C3N4 Composite. *Microchim. Acta* **2021**, *188*, 78.

(15) Freitas, M.; Nouws, H. P. A.; Delerue-Matos, C. Electrochemical Sensing Platforms for HER2-ECD Breast Cancer Biomarker Detection. *Electroanalysis* **2019**, *31*, 121−128.

(16) Nasrollahpour, H.; Isildak, I.; Rashidi, M.-R.; Hashemi, E. A.; Naseri, A.; Khalilzadeh, B. Ultrasensitive Bioassaying of HER-2 Protein for Diagnosis of Breast Cancer Using Reduced Graphene Oxide/Chitosan as Nanobiocompatible Platform. *Cancer Nanotechnol.* **2021**, *12*, 10.

(17) Augustine, S.; Kumar, P.; Malhotra, B. D. Amine-Functionalized MoO3@RGO Nanohybrid-Based Biosensor for Breast Cancer Detection. *ACS Appl. Bio Mater.* **2019**, *2*, 5366−5378.

(18) Nasrollahpour, H.; Naseri, A.; Rashidi, M.-R.; Khalilzadeh, B. Application of Green Synthesized WO3-Poly Glutamic Acid Nanobiocomposite for Early Stage Biosensing of Breast Cancer Using Electrochemical Approach. *Sci. Rep.* **2021**, *11*, 23994.

(19) Emami, M.; Shamsipur, M.; Saber, R.; Irajirad, R. An Electrochemical Immunosensor for Detection of a Breast Cancer Biomarker Based on AntiHER2-Iron Oxide Nanoparticle Bioconjugates. *Analyst* **2014**, *139*, 2858−2866.

(20) Pacheco, J. G.; Rebelo, P.; Freitas, M.; Nouws, H. P. A.; Delerue-Matos, C. Breast Cancer Biomarker (HER2-ECD) Detection Using a Molecularly Imprinted Electrochemical Sensor. *Sens. Actuators, B* **2018**, *273*, 1008−1014.

(21) Freitas, M.; Neves, M. M. P. S.; Nouws, H. P. A.; Delerue-Matos, C. Quantum Dots as Nanolabels for Breast Cancer Biomarker HER2-ECD Analysis in Human Serum. *Talanta* **2020**, *208*, 120430.

(22) Sharma, S.; Zapatero-Rodríguez, J.; Saxena, R.; O'Kennedy, R.; Srivastava, S. Ultrasensitive Direct Impedimetric Immunosensor for Detection of Serum HER2. *Biosens. Bioelectron.* **2018**, *106*, 78−85.

(23) Rauf, S.; Lahcen, A. A.; Aljedaibi, A.; Beduk, T.; Ilton de Oliveira Filho, J.; Salama, K. N. Gold Nanostructured Laser-Scribed

Graphene: A New Electrochemical Biosensing Platform for Potential Point-of-Care Testing of Disease Biomarkers. *Biosens. Bioelectron.* **2021**, *180*, 113116.
(24) Chocholova, E.; Bertok, T.; Lorencova, L.; Holazova, A.; Farkas, P.; Vikartovska, A.; Bella, V.; Velicova, D.; Kasak, P.; Eckstein, A. A.; Mosnacek, J.; Hasko, D.; Tkac, J. Advanced Antifouling Zwitterionic Layer Based Impedimetric HER2 Biosensing in Human Serum: Glycoprofiling as a Novel Approach for Breast Cancer Diagnostics. *Sens. Actuators, B* **2018**, *272*, 626−633.
(25) da Fonseca Alves, R.; Martins, I. C.; Franco, D. L.; Silva, A. d. G.; de Souza Santos, P.; Goulart, L. R.; Cristina de Paiva Maia, Y.; Faria Silva, A. T.; Gonçalves Araújo, T.; Del Pilar Taboada Sotomayor, M. A Novel Peptide-Based Electrochemical Biosensor for Breast Cancer Characterization over a Poly 3-(3-Aminophenyl) Propionic Acid Matrix. *Biosens. Bioelectron.* **2022**, *205*, 114081.
(26) Wang, W.; Han, R.; Chen, M.; Luo, X. Antifouling Peptide Hydrogel Based Electrochemical Biosensors for Highly Sensitive Detection of Cancer Biomarker HER2 in Human Serum. *Anal. Chem.* **2021**, *93*, 7355−7361.
(27) Chen, M.; Song, Z.; Han, R.; Li, Y.; Luo, X. Low Fouling Electrochemical Biosensors Based on Designed Y-Shaped Peptides with Antifouling and Recognizing Branches for the Detection of IgG in Human Serum. *Biosens. Bioelectron.* **2021**, *178*, 113016.
(28) Meng, X.; Xu, Y.; Ma, B.; Ma, Z.; Han, H. Anti-Fouling Materials Decorated Immunoprobe and Electrochemical Sensing Interface to Improve Immunoassay. *Chem. Eng. J.* **2022**, *450*, 137954.
(29) Li, M.; Lv, M.; Wang, L.; Fan, C.; Zuo, X. Engineering electrochemical interface for biomolecular sensing. *Curr. Opin. Electrochem.* **2019**, *14*, 71−80.
(30) Su, S.; Wu, Y.; Zhu, D.; Chao, J.; Liu, X.; Wan, Y.; Su, Y.; Zuo, X.; Fan, C.; Wang, L. On-Electrode Synthesis of Shape-Controlled Hierarchical Flower-Like Gold Nanostructures for Efficient Interfacial DNA Assembly and Sensitive Electrochemical Sensing of MicroRNA. *Small* **2016**, *12*, 3794−3801.
(31) Ding, H.; Yang, L.; Jia, H.; Fan, D.; Zhang, Y.; Sun, X.; Wei, Q.; Ju, H. Label-Free Electrochemical Immunosensor with Palladium Nanoparticles Functionalized MoS2/NiCo Heterostructures for Sensitive Procalcitonin Detection. *Sens. Actuators, B* **2020**, *312*, 127980.
(32) Yang, L.; Li, Y.; Zhang, Y.; Fan, D.; Pang, X.; Wei, Q.; Du, B. 3D Nanostructured Palladium-Functionalized Graphene-Aerogel-Supported Fe3O4 for Enhanced Ru(Bpy)32+-Based Electrochemiluminescent Immunosensing of Prostate Specific Antigen. *ACS Appl. Mater. Interfaces* **2017**, *9*, 35260−35267.
(33) Soleymani, L.; Fang, Z.; Sargent, E. H.; Kelley, S. O. Programming the Detection Limits of Biosensors through Controlled Nanostructuring. *Nat. Nanotechnol.* **2009**, *4*, 844−848.
(34) Love, J. C.; Wolfe, D. B.; Haasch, R.; Chabinyc, M. L.; Paul, K. E.; Whitesides, G. M.; Nuzzo, R. G. Formation and Structure of Self-Assembled Monolayers of Alkanethiolates on Palladium. *J. Am. Chem. Soc.* **2003**, *125*, 2597−2609.
(35) Chen, D.; Wang, D.; Hu, X.; Long, G.; Zhang, Y.; Zhou, L. A DNA Nanostructured Biosensor for Electrochemical Analysis of HER2 Using Bioconjugate of GNR@Pd SSs—Apt—HRP. *Sens. Actuators, B* **2019**, *296*, 126650.
(36) Huang, Y.-T.; Chang, C.-Y.; Chen, W.; Su, C.-H.; Hsu, G.-C.; Chang, C.-C. *Rapid, and Ultrasensitive Flexible Palladium Nano-Thin Film Biosensing Electrode Development for Cancer Antigen HER2 Detection*, 2017; p T1.318.
(37) Kunene, K.; Weber, M.; Sabela, M.; Voiry, D.; Kanchi, S.; Bisetty, K.; Bechelany, M. Highly-Efficient Electrochemical Label-Free Immunosensor for the Detection of Ochratoxin A in Coffee Samples. *Sens. Actuators, B* **2020**, *305*, 127438.
(38) Kim, Y.-R.; Lai, S. C. S.; McKelvey, K.; Zhang, G.; Perry, D.; Miller, T. S.; Unwin, P. R. Nucleation and Aggregative Growth of Palladium Nanoparticles on Carbon Electrodes: Experiment and Kinetic Model. *J. Phys. Chem. C* **2015**, *119*, 17389−17397.
(39) Choi, S.; Jeong, H.; Choi, K.; Song, J. Y.; Kim, J. Electrodeposition of Triangular Pd Rod Nanostructures and Their Electrocatalytic and SERS Activities. *ACS Appl. Mater. Interfaces* **2014**, *6*, 3002−3007.
(40) Shin, D. H.; Lee, J. S.; Jun, J.; An, J. H.; Kim, S. G.; Cho, K. H.; Jang, J. Flower-like Palladium Nanoclusters Decorated Graphene Electrodes for Ultrasensitive and Flexible Hydrogen Gas Sensing. *Sci. Rep.* **2015**, *5*, 12294.
(41) Zhang, J.; Feng, C.; Deng, Y.; Liu, L.; Wu, Y.; Shen, B.; Zhong, C.; Hu, W. Shape-Controlled Synthesis of Palladium Single-Crystalline Nanoparticles: The Effect of HCl Oxidative Etching and Facet-Dependent Catalytic Properties. *Chem. Mater.* **2014**, *26*, 1213−1218.
(42) Labulo, A. H.; Omondi, B.; Nyamori, V. O. Suzuki−Miyaura Reaction and Solventfree Oxidation of Benzyl Alcohol by Pd/Nitrogen-Doped CNTs Catalyst. *J. Mater. Sci.* **2018**, *53*, 15817−15836.
(43) Buijs, J.; Norde, W.; Lichtenbelt, J. W. Th. Changes in the Secondary Structure of Adsorbed IgG and F(Ab')2 Studied by FTIR Spectroscopy. *Langmuir* **1996**, *12*, 1605−1613.
(44) Salinas Domínguez, R. A.; Domínguez Jiménez, M. Á.; Orduña Díaz, A. Antibody Immobilization in Zinc Oxide Thin Films as an Easy-Handle Strategy for Escherichia Coli Detection. *ACS Omega* **2020**, *5*, 20473−20480.
(45) Mungali, M.; Singh, K. Construction of Anti Omp Immobilized Nanoporous Membrane Based Electrochemical Biosensor for the Detection of E. coli. *Global J. Multidiscip. Stud.* **2015**, *4*, 96−102.
(46) Du, D.; Zou, Z.; Shin, Y.; Wang, J.; Wu, H.; Engelhard, M. H.; Liu, J.; Aksay, I. A.; Lin, Y. Sensitive Immunosensor for Cancer Biomarker Based on Dual Signal Amplification Strategy of Graphene Sheets and Multi-Enzyme Functionalized Carbon Nanospheres. *Anal. Chem.* **2010**, *82*, 2989−2995.
(47) Darain, F.; Gan, K.; Tjin, S. Antibody Immobilization on to Polystyrene Substrate-On-Chip Immunoassay for Horse IgG Based on Fluorescence. *Biomed. Microdevices* **2009**, *11*, 653−661.
(48) Torres-González, L.; Díaz-Ayala, R.; Vega-Olivencia, C. A.; López-Garriga, J. Characterization of Recombinant His-Tag Protein Immobilized onto Functionalized Gold Nanoparticles. *Sensors* **2018**, *18*, 4262.
(49) Park, J.-E.; Park, S.-G.; Koukitu, A.; Hatozaki, O.; Oyama, N. Electrochemical and Chemical Interactions between Polyaniline and Palladium Nanoparticles. *Synth. Met.* **2004**, *141*, 265−269.
(50) Verma, S.; Singh, A.; Shukla, A.; Kaswan, J.; Arora, K.; Ramirez-Vick, J.; Singh, P.; Singh, S. P. Anti-IL8/AuNPs-RGO/ITO as an Immunosensing Platform for Noninvasive Electrochemical Detection of Oral Cancer. *ACS Appl. Mater. Interfaces* **2017**, *9*, 27462−27474.
(51) Ihalainen, P.; Majumdar, H.; Viitala, T.; Törngren, B.; Närjeoja, T.; Määttänen, A.; Sarfraz, J.; Härmä, H.; Yliperttula, M.; Österbacka, R.; Peltonen, J. Application of Paper-Supported Printed Gold Electrodes for Impedimetric Immunosensor Development. *Biosensors* **2012**, *3*, 1−17.
(52) Pacheco, F. G.; Cotta, A. A. C.; Gorgulho, H. F.; Santos, A. P.; Macedo, W. A. A.; Furtado, C. A. Comparative Temporal Analysis of Multiwalled Carbon Nanotube Oxidation Reactions: Evaluating Chemical Modifications on True Nanotube Surface. *Appl. Surf. Sci.* **2015**, *357*, 1015−1023.
(53) Tang, X.-Z.; Li, X.; Cao, Z.; Yang, J.; Wang, H.; Pu, X.; Yu, Z.-Z. Synthesis of Graphene Decorated with Silver Nanoparticles by Simultaneous Reduction of Graphene Oxide and Silver Ions with Glucose. *Carbon* **2013**, *59*, 93−99.
(54) Abdolhosseinzadeh, S.; Asgharzadeh, H.; Seop Kim, H. Fast and Fully-Scalable Synthesis of Reduced Graphene Oxide. *Sci. Rep.* **2015**, *5*, 10160.
(55) Badea, M. Simple Surface Functionalization Strategy for Immunosensing Detection of Aflatoxin B1. *Int. J. Electrochem. Sci.* **2016**, *11*, 6719−6734.
(56) Meng, L.; Jin, J.; Yang, G.; Lu, T.; Zhang, H.; Cai, C. Nonenzymatic Electrochemical Detection of Glucose Based on Palladium-Single-Walled Carbon Nanotube Hybrid Nanostructures. *Anal. Chem.* **2009**, *81*, 7271−7280.

https://doi.org/10.1021/acsomega.2c03532
ACS Omega 2022, 7, 34177−34189

(57) Chang, Z.; Fan, H.; Zhao, K.; Chen, M.; He, P.; Fang, Y. Electrochemical DNA Biosensors Based on Palladium Nanoparticles Combined with Carbon Nanotubes. *Electroanalysis* **2008**, *20*, 131−136.
(58) Biswas, S.; Lan, Q.; Xie, Y.; Sun, X.; Wang, Y. Label-Free Electrochemical Immunosensor for Ultrasensitive Detection of Carbohydrate Antigen 125 Based on Antibody-Immobilized Biocompatible MOF-808/CNT. *ACS Appl. Mater. Interfaces* **2021**, *13*, 3295−3302.
(59) Li, J.; Liu, S.; Yu, J.; Lian, W.; Cui, M.; Xu, W.; Huang, J. Electrochemical Immunosensor Based on Graphene−Polyaniline Composites and Carboxylated Graphene Oxide for Estradiol Detection. *Sens. Actuators, B* **2013**, *188*, 99−105.
(60) Solanki, P.; Kaushik, A.; Ansari, A.; Tiwari, A.; Malhotra, B. Multi-Walled Carbon Nanotubes/Sol−Gel-Derived Silica/Chitosan Nanobiocomposite for Total Cholesterol Sensor. *Sens. Actuators, B* **2009**, *137*, 727−735.
(61) Chen, A.; Ostrom, C. Palladium-Based Nanomaterials: Synthesis and Electrochemical Applications. *Chem. Rev.* **2015**, *115*, 11999−12044.
(62) Yuan, Y.; Li, L.; Zhao, M.; Zhou, J.; Chen, Z.; Bai, L. An Aptamer Based Voltammetric Biosensor for Endotoxins Using a Functionalized Graphene and Molybdenum Disulfide Composite as a New Nanocarrier. *Analyst* **2019**, *144*, 1253−1259.
(63) Weber, S. G.; Long, J. T. Detection Limits and Selectivity in Electrochemical Detectors. *Anal. Chem.* **1988**, *60*, 903A−913A.

https://doi.org/10.1021/acsomega.2c03532
ACS Omega 2022, 7, 34177−34189